Mohammadiun, H., *et al.*: Axisymmetric Stagnation-Point Flow and Heat ...
THERMAL SCIENCE: Year 2019, Vol. 23, No. 5B, pp. 3153-3164

3153

AXISYMMETRIC STAGNATION-POINT FLOW AND HEAT TRANSFER OF NANOFLUID IMPINGING ON A CYLINDER WITH CONSTANT WALL HEAT FLUX

by

Hamid MOHAMMADIUN[a], Vahid AMERIAN[b], Mohammad MOHAMMADIUN[a], Iman KHAZAEE[c], Mohsen DARABI[d*], and Mohammadreza ZAHEDI[d]

[a] Department of Mechanical Engineering, Shahrood Branch,
Islamic Azad University, Shahrood, Iran
[b] Department of Mechanical Engineering, Shahrood University, Shahrood, Iran
[c] Faculty of Mechanical and Energy Engineering,
Shahid Beheshti University, Tehran, Iran
[d] Young Researchers and Elite Club, Shahrood Branch,
Islamic Azad University, Shahrood, Iran

The steady-state, viscous flow and heat transfer of nanofluid in the vicinity of an axisymmetric stagnation point of a stationary cylinder with constant wall heat flux is investigated. The impinging free-stream is steady and with a constant strain rate, $\bar{k}$. Exact solution of the Navier-Stokes equations and energy equation are derived in this problem. A reduction of these equations is obtained by use of appropriate transformations introduced in this research. The general self-similar solution is obtained when the wall heat flux of the cylinder is constant. All the previous solutions are presented for Reynolds number $Re = \bar{k}a^2/2v_f$ ranging from 0.1 to 1000, selected values of heat flux and selected values of particle fractions where a is cylinder radius and v_f is kinematic viscosity of the base fluid. For all Reynolds numbers, as the particle fraction increases, the depth of diffusion of the fluid velocity field in radial direction, the depth of the diffusion of the fluid velocity field in z-direction, shear-stresses and pressure function decreases. However, the depth of diffusion of the thermal boundary-layer increases. It is clear by adding nanoparticles to the base fluid there is a significant enhancement in Nusselt number and heat transfer.

Key words: *nanofluid, stagnation-point flow, heat transfer, Nusselt number,
stationary cylinder, self-similar solution*

Introduction

In recent years, many researchers have been performed to study the effects of nanofluid on convective heat transfer rate. Sheikholeslami and Shehzad [1] reported the numerical analysis of Fe_3O_4-H_2O nanofluid-flow in permeable media under the effect of external magnetic source. Sheikholeslami and Seyednezhad [2] has obtained the numerical solution for nanofluid electrohydrodynamic flow and natural-convection heat transfer in a porous medium. Also they considered thermal radiation term in energy equation. In other research Sheikholeslami [3] investigated the homogeneous nanofluid-flow and forced convection heat transfer inside a lid driven porous cavity. In this work influence of Lorentz forces and shape effect of nanoparticle

---

on nanofluid MHD forced convection have been considered and temperature distribution and flow style have been presented for various values of Hartmann, Darcy, and Reynolds numbers.

Sheikholeslami *et al.* [4] presented numerical simulation for heat transfer intensification of nanofluid in a porous curved enclosure considering shape effect of Fe_3O_4 nanoparticles Sheikholeslami [5] reported magnetic field influence on nanofluid thermal radiation in a cavity with tilted elliptic inner cylinder.

The history of the analytical methods studies using similarity solution techniques goes back to Hiemenz [6]. Wang [7] was first who found exact solution for the problem of axisymmetric stagnation flow on an infinite stationary circular cylinder. Gorla [8-11] in a series of papers, studied the steady and unsteady flows over a circular cylinder in the vicinity of the stagnation-point for the cases of constant axial movement, and the special case of axial harmonic motion of a non-rotating cylinder. This special case is only for small and high values of frequency parameter using perturbation techniques.

Mohammadiun *et al.* [12] have investigated the stagnation-point flow and heat transfer of a viscous, compressible fluid on a cylinder, and in the next study the problem of stagnation point flow and heat transfer of compressible fluid impinging on a moving cylinder has been considered by them [13]. They continued their investigation by solving the problem of stagnation point flow of a nanofluid on stationary cylinder when the wall temperature of the cylinder was constant [14].

The MHD mixed convection slip flow near a stagnation-point on a non-linearly vertical stretching sheet in the presence of viscous dissipation has been considered by shateyi and mabood [15].

Mahmood *et al.* [16] has been discussed the time-dependent axisymmetric stagnation-point flow and heat transfer of a viscous fluid over a disc lubricated with power-law fluid. The aim of their study was to investigate the influence of slip parameter and unsteadiness parameter on the flow characteristics and heat transfer.

Amirsom *et al.* [17] presented the similarity solution of governing equations for the magneto convective stagnation point flow of bionanofluid with melting heat transfer. A lattice Boltzmann model of nanofluid flow boiling in a tube has been established by Yao *et al.* [18]. They simulated the effect of different bubble distances and lateral accelerations a on the bubble growth process and the effect of heat transfer.
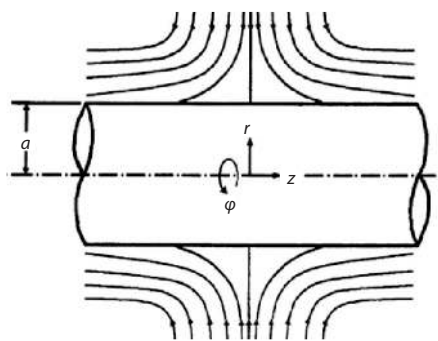
In the present analysis, for the first time the similarity solution of the heat transfer enhancement of steady viscous flow of nanofluid in the vicinity of an axisymmetric stagnation point of a stationary cylinder with constant heat flux is considered. It is interesting to note that in current work the thermal conductivity coefficient of nanofluid is considered temperature-dependent and the ODE has been derived. Flow is considered in cylindrical co-ordinate (r, z) with corresponding velocity u and w components, as fig. 1. The laminar steady incompressible flow of nanofluid in the neighborhood of an axisymmetric stagnation-point of a stationary cylinder is considered.

Figure 1. Schematic diagram of a stationary cylinder

Properties of nanofluid

The aluminum oxide, γAl_2O_3, nanoparticles which have been used in this research have the following characteristics:

Density $\rho_m = 3600$ kg/m^3, mean particle diameter is 44 nm.

Density

We will assume that the density of the Al_2O_3 nanoparticles is constant in the entire range of considered temperature. The following relation has been used to compute the nanofluid density:

$$\rho_n = (1 - \phi_v)\rho_f + \phi_v \rho_p \tag{1}$$

where subscripts n, f, and p denote the nanofluid, base fluid, and the particles, respectively, and ϕ_v is the particle fraction.

Dynamic viscosity

Corcione [19] proposed empirical correlation for predicting the relative viscosity:

$$\frac{\mu_n}{\mu} = \frac{1}{1 - 34.87 \left(\dfrac{d_p}{d_f}\right)^{-0.3} \phi_v^{1.03}} \tag{2}$$

where d_f is the equivalent diameter of a base fluid molecule:

$$d_f = 0.1 \left(\frac{6M}{N\pi\rho_{f0}}\right)^{1/3} \tag{3}$$

where M is the molecular weight of the base liquid, N – the Avogadro number, and ρ_{f0} – the mass density of the base liquid calculated at temperature $T_0 = 293$ K.

Different values used in this formula are mentioned in tab. 1.

Table 1. Different parameters of nanofluid and base fluid

Parameter	Value
Thermal conductivity of base fluid, k_f	0.6316 [Wm^{-1}K^{-1}]
Thermal conductivity of nanoparticle, k_p	40 [Wm^{-1}K^{-1}]
Specific heat of base fluid, $C_{p,f}$	4.181 [kJkg^{-1}K^{-1}]
Specific heat of nanoparticle, $C_{p,p}$	0.765 [kJkg^{-1}K^{-1}]
Density of base fluid, ρ_f	987.6 [kgm^{-3}]
Density of nanoparticle, ρ_p	3600 [kgm^{-3}]
Viscosity of base fluid, μ_f	0.000538 [kgm^{-1}s^{-1}]
Diameter of nanoparticle, d_p	44 [nm]
Diameter of base fluid molecule, d_f	0.384 [nm]

In this research Corcione's formula has been used to extract the Navier-Stocks equations.

Thermal conductivity

Two different models have been used to determine the thermal conductivity coefficient of nanofluid.

Model 1

Corcione [19] proposed empirical correlation for predicting the effective thermal conductivity based on a high number of experimental data available in the literature. It is found that, for given the nanoparticle material and the base fluid, the ratio between the thermal conductivities of the nanofluid and the pure base liquid increases as the nanoparticle volume fraction and the temperature are increased, and the nanoparticle diameter is decreased. The ease of application of the equations proposed, and their wide regions of validity for the thermal conductivity data, make such equations useful by the engineering point of view, for both numerical simulation purposes and thermal design tasks:

$$\frac{k_{\text{eff}}}{k_f} = 1 + 4.4 \, \text{Re}_p^{\,0.4} \, \text{Pr}_{bf}^{\,0.66} \left(\frac{T}{T_{fr}} \right)^{10} \left(\frac{k_p}{k_f} \right)^{0.03} \varphi_v^{\,0.66} \tag{4}$$

where T_{fr} is the freezing point unit of the base fluid. Also Re_p and Pr_{bf} are the nanoparticle Reynolds number and the base fluid Prandtl number, respectively, presented:

$$\text{Re}_p = \frac{2\rho_{bf} k_b T}{\pi \mu_{bf}^{\,2} d_p} \quad \text{and} \quad \text{Pr}_{bf} = \frac{\mu_{bf}(c_p)_{bf}}{k_{bf}} \tag{5}$$

where k_b is the Boltzmann's constant equal to $1.38066 \cdot 10^{-23}$ J/K. Finally, the Corcione's correlation, which is temperature-dependent correlation, has been used to extract the energy equation.
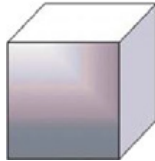
Model 2

In Model 2 thermal conductivity coefficient of nanofluid has been expressed by following relation [2, 3]:

$$\frac{k_{\text{eff}}}{k_f} = \frac{-m(k_f - k_p)\phi_v + (k_p - k_f)\phi_N + mk_f + k_p + k_f}{mk_f + (k_f - k_p)\phi_v + k_f + k_p} \tag{6}$$

Values of shape factors for various shapes of nanoparticles are presented in tab. 2.

Table 2. The values of shape factor of different shapes of nanoparticles [2]

Spherical		3
Platelet		5.7
Cylinder		4.8
Brick		3.7

Mohammadiun, H., *et al.*: Axisymmetric Stagnation-Point Flow and Heat ...
THERMAL SCIENCE: Year 2019, Vol. 23, No. 5B, pp. 3153-3164

3157

Problem formulation

The laminar steady incompressible flow of nanofluid in the neighborhood of an axisymmetric stagnation-point of a stationary cylinder has been considered. The Navier-Stokes and energy equations in cylindrical co-ordinates governing the axisymmetric flow are given by [7-11]:

– mass

$$\frac{\partial}{\partial r}(ru) + r\frac{\partial w}{\partial z} = 0 \tag{7}$$

– momentum

$$u\frac{\partial u}{\partial r} + w\frac{\partial u}{\partial z} = -\frac{1}{\rho_n}\frac{\partial p}{\partial r} + \nu_n\left(\frac{\partial^2 u}{\partial r^2} + \frac{1}{r}\frac{\partial u}{\partial r} - \frac{u}{r^2} + \frac{\partial^2 u}{\partial z^2}\right) \tag{8}$$

$$u\frac{\partial w}{\partial r} + w\frac{\partial w}{\partial z} = -\frac{1}{\rho_n}\frac{\partial p}{\partial z} + \nu_n\left(\frac{\partial^2 w}{\partial r^2} + \frac{1}{r}\frac{\partial w}{\partial r} + w\frac{\partial^2 w}{\partial z^2}\right) \tag{9}$$

– energy

$$\frac{1}{r}\frac{\partial}{\partial r}\left(rk_{\text{eff}}\frac{\partial T}{\partial r}\right) + \frac{\partial}{\partial z}\left(k_{\text{eff}}\frac{\partial T}{\partial z}\right) = (\rho c_p)_n\left[u\frac{\partial T}{\partial r} + w\frac{\partial T}{\partial z}\right] \tag{10}$$

The boundary conditions for velocity field:

$$r = a: \quad u = 0, \quad w = 0 \tag{11}$$

$$r \to \infty: \quad u = -\overline{k}\left(r - \frac{a^2}{r}\right), \quad w = 2\overline{k}z \tag{12}$$

In which, eq. (11) are no-slip conditions on the cylinder wall and relations eq. (12) show that the viscous flow solution approaches, in an analogous manner to the Hiemenz flow, the potential flow solution as $r \to \infty$. For the temperature field:

$$\begin{cases} r = a: \quad q = q_{} = \text{constant} \\ \\ r \to \infty \quad T \to T_\infty \end{cases} \tag{13}$$

where q_w is the wall heat flux, respectively, and T_∞ – the freestream temperature.

A reduction of the Navier-Stokes equations is obtained by the following co-ordinate separation of the velocity field which is actually modeled by the form of their limits:

$$u = -\overline{k}\frac{a}{\sqrt{\eta + 1}}f(\eta), \quad w = 2\overline{k}f'(\eta)z, \quad p = \rho_n\overline{k}^2 a^2 P \tag{14}$$

where $\eta = (r/a)^2 - 1$ is dimensionless radial variable and prime denotes differentiation with respect to η. Transformations eq. (14) satisfy eq. (7) automatically and their insertion into eqs. (8)-(10) yields an ODE in terms of $f(\eta)$, and an expression for the pressure:

$$(\eta + 1)f''' + f'' + \text{Re}_n\left[1 - (f')^2 + ff''\right] = 0 \tag{15}$$

$$P - P_0 = -\left[\frac{f^2(\eta)}{2(\eta + 1)} + \frac{1}{\text{Re}_n}f'(\eta)\right] - 2\left(\frac{z}{a}\right)^2 \tag{16}$$

In these equations:

$$\text{Re}_n = \beta \frac{\overline{k}a^2}{2v_f} \tag{17}$$

$$\beta = \left[1 - 34.87\left(\frac{d_p}{d_f}\right)^{-0.3} \phi_v^{1.03}\right]\left(1 - \phi_v + \phi_v \frac{\rho_p}{\rho_f}\right) \tag{18}$$

and Re_n is the Reynolds number for nanofluid. From conditions eqs. (11) and (12), the boundary conditions for eq. (14):

$$\eta = 0: \quad f = 0, \quad f' = 0$$
$$\eta \to \infty: \quad f' = 1 \tag{19}$$

To transform the energy equation into a non-dimensional form, we introduce:

$$\theta(\eta) = \frac{T(\eta) - T_\infty}{\dfrac{aq_w}{2k_{bf}}} \tag{20}$$

By using Corcione's correlation and introducing Γ:

$$\Gamma = 4.4\left(\frac{2\rho_{bf}K_b}{\pi\mu_{bf}^2 d_p}\right)^{0.4} \frac{1}{T_{fr}^{10}}\left(\frac{k_p}{k_f}\right)^{0.03} \tag{21}$$

The energy equation can be written:

$$\left\{1 + \Gamma\phi_v^{0.66}\text{Pr}_{bf}^{0.66}\left[T_\infty + \frac{aq_w}{2k_{bf}}\theta\right]^{10.4}\right\}[(\eta+1)\theta'' + \theta'] + 10.4\left[T_\infty + \frac{aq_w}{2k_{bf}}\theta\right]^{9.4} \cdot$$
$$\cdot\frac{aq_w}{2k_{bf}}\Gamma\phi_v^{0.66}\text{Pr}_{bf}^{0.66}(\eta+1)(\theta')^2 + \left\{1 - \phi_v + \phi_v\left[\frac{(\rho c_p)_p}{(\rho c_p)_f}\right]\right\}\text{Re}_{bf}\text{Pr}_{bf}f\theta' = 0 \tag{22}$$

Using *Model 2* of thermal conductivity coefficient leads to following relation for energy equation:

$$(\eta+1)\theta'' + \theta' + \text{Re}_n\text{Pr}_{nf}f\theta' = 0 \tag{23}$$

From condition eq. (13), the boundary conditions for eqs. (22) and (23):

$$\begin{cases} \eta = 0: \quad -\dfrac{k_{nf}}{k_{bf}}\theta'(0) = 1 \\ \eta \to \infty: \quad \theta(\infty) = 0 \end{cases} \tag{24}$$

Equations (15), (22), and (23) along with boundary conditions eqs. (19) and (24) have been solved by using the finite difference method along with TDMA algorithm [20]. Using this method, the initial values were guessed and the iteration was repeated until the convergence was obtained. In these computations the grid size was chosen 0.001 and the truncation error was set at 1E-9.

The flowchart of numerical method was depicted in the *Appendix*.

Nusselt number

The Nusselt number has been presented by the following relations:

Mohammadiun, H., *et al.*: Axisymmetric Stagnation-Point Flow and Heat ...
THERMAL SCIENCE: Year 2019, Vol. 23, No. 5B, pp. 3153-3164

3159

$$\theta(0) = \frac{T_w - T_\infty}{\dfrac{aq_w}{2k_{bf}}} \quad \text{and} \quad h = \frac{q_w}{T_w - T_\infty} \rightarrow \text{Nu} = \frac{ha}{2k_{bf}} = \frac{1}{\theta(0)} \tag{25}$$

Shear-sress

The shear-stress on the surface of the cylinder is obtained from:

$$\sigma = \mu_n \left[\frac{\partial w}{\partial r} \right]_{r=a} \tag{26}$$

where μ_n is viscosity of the nanofluid. Using definition (14), the shear-stress at the cylinder wall for self-similar solutions becomes:

$$\sigma = \mu_n [2\bar{k}f''(0)z]\frac{2}{a} \Rightarrow \frac{\sigma a}{4\mu_n \bar{k}z} = f''(0) \tag{27}$$

Results and discussions

In this section, the solution of the ODE (15) and (22), for prescribed values of surface heat flux and selected values of Reynolds numbers and particle volume fraction are presented.

Sample profiles of the $f(\eta)$ function against η at $\phi_v = 0.02$ and for selected values of Reynolds numbers are presented in fig. 2. Since with the increase of Reynolds number the dynamic inertia forces overcome the viscosities forces, as expected like the behavior of the base fluid, the depth of diffusion of the momentum increases. So as the Reynolds number increases, the depth of diffusion of the fluid velocity field in radial direction increases, too.

Effects of variation of particle volume fraction factor on $f(\eta)$ function against η and selected value of Reynolds number Re = 1000 is shown in fig. 3. Since any increase of ϕ_v leads to an increase in dynamic viscosity, the resistance of the viscos forces against the dynamic inertia forces increases. It is interesting to note that as ϕ_v increases the depth of diffusion of the fluid velocity field in radial direction decreases. So, for all the Reynolds numbers, the base fluid case produces the highest value of radial velocity and as particle Volume fraction increases, this quantity decreases accordingly.
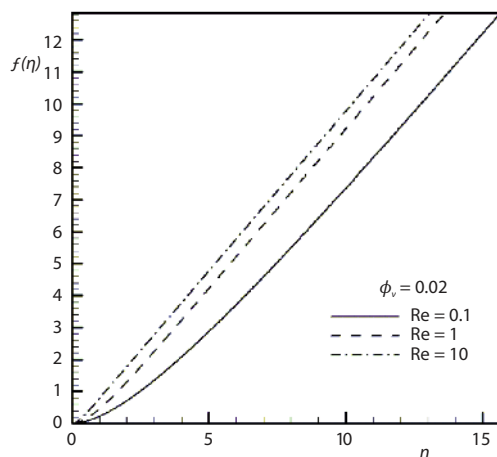

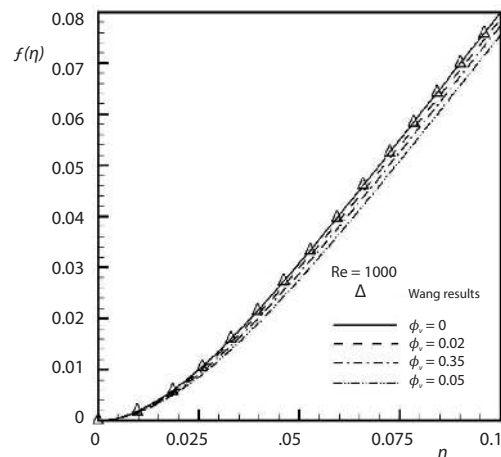**Figure 2. Variation of *f* in terms of *η* at $\phi_v = 0.02$ for different values of Reynolds number**

Figure 3. Variation of *f* in terms of *η* at Re = 1000 and for different values of particle volume fraction

3160

Mohammadiun, H., *et al.*: Axisymmetric Stagnation-Point Flow and Heat ...
THERMAL SCIENCE: Year 2019, Vol. 23, No. 5B, pp. 3153-3164

Sample profiles of the $f'(\eta)$ function against η for $\phi_v = 0.02$, and for selected values of Reynolds numbers are shown in fig. 4. Again as Reynolds number increases, the depth of diffusion of the fluid velocity field in z-direction increases, too.

Effects of variations of particle volume fraction factor on $f'(\eta)$ function against η for selected value of Reynolds number Re = 0.1 are shown in fig. 5. It is interesting to note that as ϕ_v increases the depth of the diffusion of the fluid velocity field in z-direction also decreases. Again, the base fluid case, $\phi_v = 0$, produces the highest value of velocity in z-direction and as particle volume fraction factor increases, this quantity decreases accordingly.
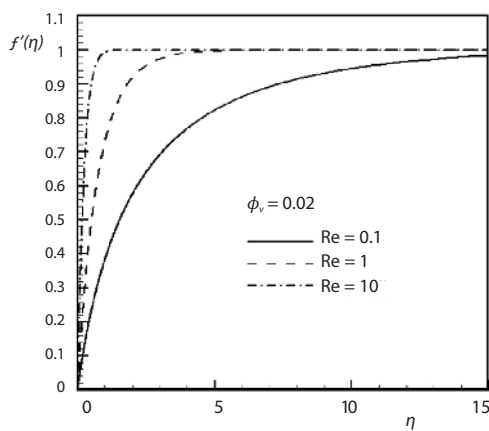

Figure 4. Variation of f' in terms of η at $\phi_v = 0.02$ at and for different values of Reynolds number
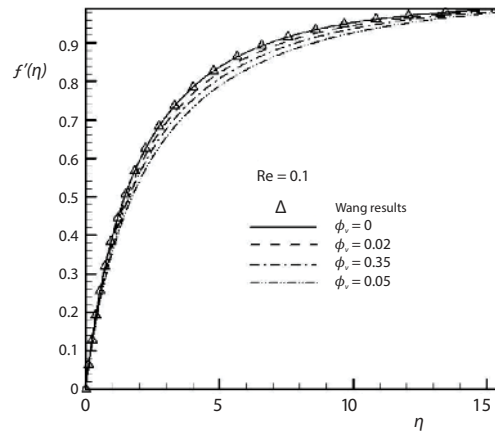

Figure 5. Variation of f' in terms of η at Re = 0.1 and for different values of particle volume fraction

Sample profiles of the $\theta(\eta)$ function against η for the case of constant wall heat flux for $\phi_v = 0.05$, $aq_w/2k_{bf} = 200$, and for selected values of Reynolds numbers are depicted in fig. 6. As expected, the momentum is increased with the Reynolds number and consequently, not only the thermal boundary-layer thickness is decreased once the thermal diffusion is overcome, but also the wall dimensionless temperature is decreased, as can be observed in the following figures.
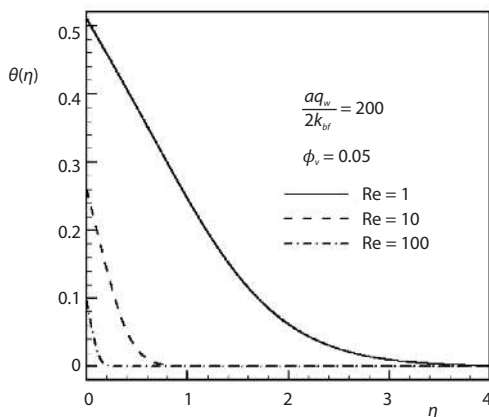

Figure 6. Variation of $\theta(\eta)$ in terms of η at $aq_w/2k_{bf} = 200$ and $\phi_v = 0.05$ for different values of Reynolds number
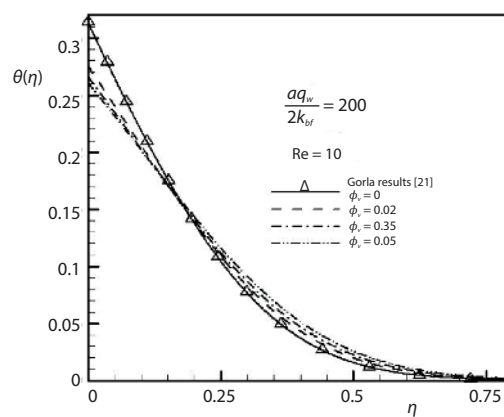

Figure 7. Variation of $\theta(\eta)$ in terms of η at $aq_w/2k_{bf} = 200$ and Re = 10 for different values of particle fractions

Effect of variations of particle fraction factor on $\theta(\eta)$ function against η for, $aq_w/2k_{bf}$ = constant, and selected values of Reynolds numbers are presented in figs. 7 and 8. For $\phi_v = 0$, base fluid, the result of Gorla [21] is extracted; it is interesting to note that, as ϕ_v increases, the absolute value of the dimensionless temperature gradient is decreased at surfaces and the wall dimensionless temperature is decreased, too; nevertheless, this decreasing rate is negligible compared to that of the heat transfer coefficient. Therefore, the heat transfer coefficient is increased through addition of nanoparticles.

Sample profiles of the dimensionless temperature $\theta(\eta)$ against η for $\phi_v = 0.05$ and Re = 100, for selected values of heat flux are depicted in fig. 9. As heat flux increases, the dimensionless temperature decreases and so does the temperature gradient at surface. It is evident that the absolute value of the dimensionless temperature gradient is decreased at surfaces; nevertheless, this decreasing rate is negligible compared to that of the heat transfer coefficient. Therefore, the Nusselt number is increased through addition of nanoparticles.
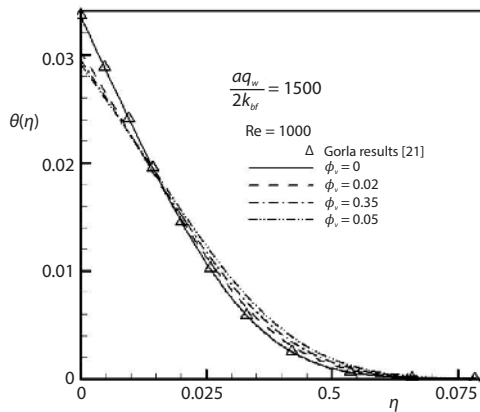

Figure 8. Variation of $\theta(\eta)$ in terms of η at $aq_w/2k_{bf}$ = 1500 and Re = 1000 for different values of particle fractions
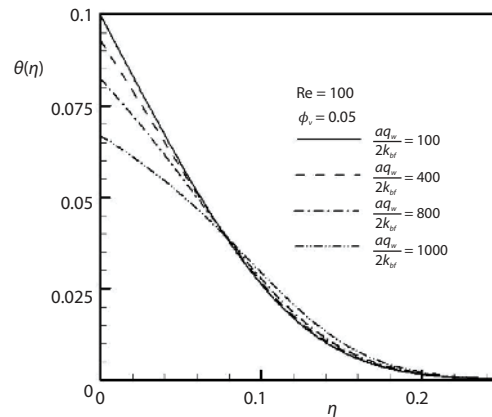
Figure 9. Variation of $\theta(\eta)$ in terms of η at $\phi_v = 0.05$ and Re = 100 for different values of $aq_w/2k_{bf}$

Effects of variations of particle fraction factor on Nusselt number against Reynolds number for selected values of wall heat flux are presented in fig. 10. It is interesting to note that, as ϕ_v increases, the depth of the diffusion of the thermal boundary-layer increases. Based on the figures, an increase in the heat flux and the Reynolds number along with addition of nanoparticles will result in increased heat transfer coefficient.

Effect of wall heat flux on Nusselt number against Reynolds number for selected values of variations of particle fraction factor is depicted in fig. 11. As it reveals in this figures, increase in heat flux results in decrease in dimensionless temperature at the surface, whereas Nusselt number has inverse relation with dimensionless temperature at surface, as heat flux increases Nusselt number increases as well. Generally more heat flux results in more temperature gradient at the surface, also forced heat convection increases same as the heat convection coefficient.

Sample profiles of non-dimensional temperature, derived by using eq. (25) for thermal conductivity are shown in fig. 12. As it is clear, both employed model in this research are showing same trend, which validates how useful the first model is. The profiles reveal that as shape factor increases, temperature at surface decreases. Whereas, considering reverse relation
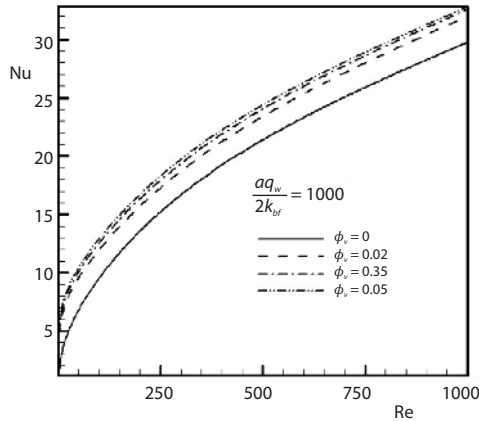
Figure 10. Variation of Nusselt number in terms of Reynolds number at $aq_w/2k_{bf} = 1000$ for different values of particle fractions
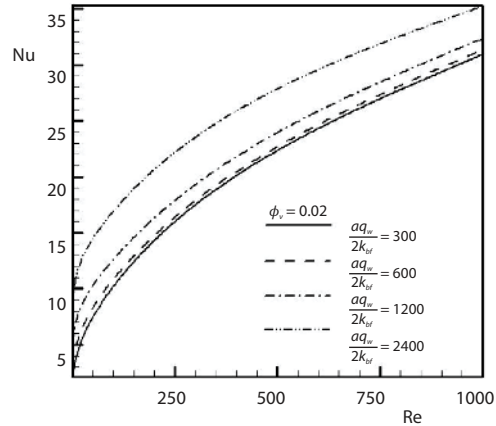

Figure 11. Variation of Nusselt number in terms of Reynolds number at $\phi_v = 0.02$ for different values of $aq_w/2k_{bf}$

between Nuselt number and temperature, an increase in shape factor results in an increase in Nuselt number. Therefore, platelet particles are more effective than spherical ones in enhancement of heat transfer.

In fig. 13, effect of particle volume fraction on dimensionless temperature is shown. Sample profiles are plotted using eq. (25) for thermal conductivity. As it is expected, same as the trend in figs. 7 and 8, the more particle volume fraction, the less non-dimensional temperature at surface and consequently more Nuselt number.
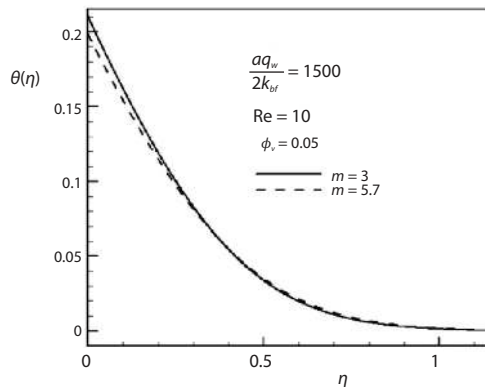

Figure 12. Variation of $\theta(\eta)$ in terms of η at $aq_w/2k_{bf} = 1500$ and Re = 10 for different values of shape factor
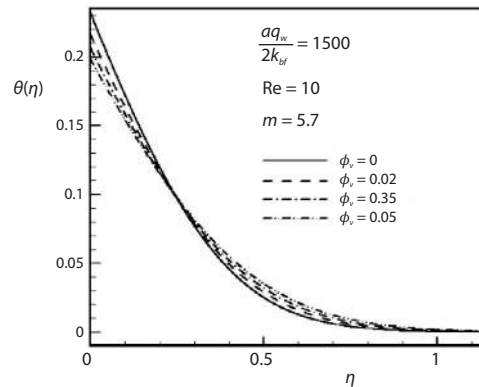
Figure 13. Variation of $\theta(\eta)$ in terms of η at $aq_w/2k_{bf} = 1500$ and Re = 10 for different values of particle fractions

Conclusion

A similarity solution for the Navier-Stokes equations and energy equation has been obtained for the problem of axisymmetric stagnation-point flow of a nanofluid on a stationary cylinder with constant wall heat flux. A reduction of these equations is obtained by the use of appropriate transformations introduced for the first time. The general self-similar solution is obtained when the wall heat flux of the cylinder is constant. All the previous solutions have

Mohammadiun, H., *et al.*: Axisymmetric Stagnation-Point Flow and Heat ...
THERMAL SCIENCE: Year 2019, Vol. 23, No. 5B, pp. 3153-3164

3163

been presented for Reynolds numbers, $\mathrm{Re} = \bar{k}\,a^2/2\nu_f$ ranging from 0.1-1000 and different values of particle volume fraction. It can be said that for all Reynolds numbers and cylinder wall heat flux, as increases the depth of diffusion of the fluid velocity field in radial and axial directions decreases. But the Nusselt number and the depth of diffusion of the thermal boundary-layer increases.

Nomenclature

a – radius of the cylinder, [m]
d_f – equivalent diameter of a base fluid molecule, [m]
d_p – equivalent diameter of a particle molecule, [m]
f – dimensionless function, [–]
h – convective heat transfer coefficient, [Wm^{-2}K^{-1}]
$\bar{k}$ – strain rate of free stream, [s^{-1}]
k_{eff} – thermal conductivity of nanofluid, [Wm^{-1}K^{-1}]
m – shape factor, [–]
Nu – Nusselt number
Pr_b – base fluid Prandtl number
P – dimensionless pressure, [–]
q_w – wall heat flux, [Wm^{-2}]
Re – base fluid Reynolds number
Re_n – nanofluid Reynolds number
Re_p – nanoparticle Reynolds number

r, z – cylindrical co-ordinates, [m]
T_{fr} – the freezing point unit of the base fluid, [K]
u – radial component of velocity field, [ms^{-1}]
w – axial component of velocity field, [ms^{-1}]

Greek symbols

η – similarity variable, [–]
θ – dimensionless temperature, [–]
μ_n – dynamic viscosity of the nanofluid, [kgm^{-1}s^{-1}]
μ – dynamic viscosity of the base fluid, [kgm^{-1}s^{-1}]
ν_f – kinematic viscosity of base fluid, [ms^{-1}]
ν_n – kinematic viscosity of nanofluid, [m^{2}s^{-1}]
ρ – nanofluid density, [kgm^{-2}]
ρ_f – base fluid density, [kgm^{-2}]
ρ_p – particle density, [kgm^{-2}]
σ – shear stress, [kgm^{-1}s^{-2}]
ϕ_v – particle fraction, [–]

References

[1] Sheikholeslami, M., Shehzad, S. A., Numerical Analysis of Fe$_3$O$_4$-H$_2$O Nanofluid-Flow in Permeable Media under the Effect of External Magnetic Source, *International Journal of Heat and Mass Transfer, 118* (2018), Mar., pp. 182-192

[2] Sheikholeslami, M., Seyednezhad, M., Simulation of Nanofluid Flow and Natural-Convection in a Porous Media under the Influence of Electric Field Using CVFEM, *International Journal of Heat and Mass Transfer*, *120* (2018), May, pp. 772-781

[3] Sheikholeslami, M., CuO-water Nanofluid Flow Due to Magnetic Field Inside a Porous Media Considering Brownian Motion, *Journal of Molecular Liquids*, *249* (2018), Jan., pp. 921-929

[4] Sheikholeslami, M., *et al*., Numerical Simulation for Heat Transfer Intensification of Nanofluid in a Porous Curved Enclosure Considering Shape Effect of Fe$_3$O$_4$ Nanoparticles, *Chemical Engineering and Processing*: *Process Intensification*, *124* (2018), Feb., pp. 71-82

[5] Sheikholeslami, M., Magnetic Field Influence on Nanofluid Thermal Radiation in a Cavity with Tilted Elliptic Inner Cylinder, *Journal of Molecular Liquids*, *229* (2017), Mar., pp. 137-147

[6] Hiemenz, K., Die Grenzchicht an einem in den gleichformingen Flussigkeitsstrom eingetauchten geraden, Kreiszylinder, *Dinglers Polytech. J.*, *326* (1911), pp. 321-410

[7] Wang, C., Axisymmetric Stagnation Flow on a Cylinder, Quarterly of Applied Mathematics, *32* (1974), 2, pp. 207-213

[8] Gorla, R. S. R., Unsteady Laminar Axisymmetric Stagnation Flow over a Circular Cylinder, *Dev. Mech*, *9* (1977), pp. 286-288

[9] Gorla, R. S. R., Non-Similar Axisymmetric Stagnation Flow on a Moving Cylinder, *Int. J. Engineering Science*, *16* (1978), 6, pp. 397-400

[10] Gorla, R. S. R., Transient Response Behavior of an Axisymmetric Stagnation Flow on a Circular Cylinder Due to Time Dependent Free Stream Velocity, *Int. J. Engng. Sci, 16* (1978), 7, pp. 493- 502

[11] Gorla, R. S. R., Unsteady Viscous Flow in the Vicinity of an Axisymmetric Stagnation-Point on a Cylinder, *Int. J. Engng. Sci, 17* (1979), 1, pp. 87-93

[12] Mohammadiun, H., Rahimi, A. B., Stagnation-Point Flow and Heat Transfer of a Viscous, Compressible Fluid on a Cylinder, *Journal of Thermophysics and Heat Transfer*, *26* (2012), 3, pp. 494-502

3164

Mohammadiun, H., *et al.*: Axisymmetric Stagnation-Point Flow and Heat ...
THERMAL SCIENCE: Year 2019, Vol. 23, No. 5B, pp. 3153-3164

[13] Rahimi, A. B., *et al.*, Axisymmetric Stagnation Flow and Heat Transfer of a Compressible Fluid Imping-ing on a Cylinder Moving Axially, *Journal Heat Transfer*, *138* (2016), 2, 022201

[14] Mohammadiun, H., *et al.*, Similarity Solution of Axisymmetric Stagnation-Point Flowand Heat Transfer of a Nanofluid on a Stationary Cylinderwith Constant Wall Temperature, *Iran J. Sci. Technol Trans. Mech. Eng.*, *41* (2017), 1, pp. 91-95

[15] Shateyi, S., Mabood, F., The MHD Mixed Convection Slip Flow Near a Stagnation-Point on a Non-Lin-early Vertical Stretching Sheet in the Presence of Viscous Dissipation, *Thermal Science*, *21* (2017), 6B, pp. 2731-2745

[16] Mahmood, K., *et al.*, Heat Transfer Analysis in the Time-Dependent Axisymmetric Stagnation Point Flow over a Lubricated Surface, *Thermal Science*, *22* (2018), 6, pp. 2483-2492

[17] Amirsom, N., *et al.*, Electro Magneto Convective Stagnation Point Flow of Bionanofluid with Melting Heat Transfer and Stefan Blowing, *Thermal Science*, *22* (2018), 6, pp. 2871-2881

[18] Yao, S., *et al.*, Simulation of Flow Boiling of Nanofluid in Tube Based on LBM, *Thermal Science*, *23* (2019), 1, pp. 159-168

[19] Corcione, M., Empirical-Correlating Equations for Predicting the Effective Thermal Conductivity and Dynamic Viscosity of Nanofluids, *Ene. Convers. Manage*, *52* (2011), 1, pp. 789-793

[20] Press, W. H, *et al.*, *Numerical Recipes*: *The Art of Scientific Computing*, Cambridge Univ. Press, New York, USA, 1997

[21] Gorla, R. S. R., Heat Transfer in an Axisymmetric Stagnation Flow on a Cylinder, *Applied Scientific Re-search*, *32* (1976), 5, pp. 541-553

Appendix